Dedicated to Acad. Aureliu Săndulescu's 75th Anniversary

VARIOUS ASPECTS OF NUCLEAR THERMODYNAMICS

A. H. RĂDUȚĂ[1,2]

[1] LNS-INFN, I-95123, Catania, Italy
[2] NIPNE, RO-76900 Bucharest, Romania
E-mail: raduta@lns.infn.it

Received March 27, 2007

Various aspects of the nuclear multifragmentation phenomenon and its link to nuclear thermodynamics are discussed. Most of the studies included herein are performed within the microcanonical multifragmentation model (MMM), a model which provided over the time very good description of the available experimental multifragmentation data. As will be seen, this model predicts a first order phase transition in nuclear matter. This transition is influenced by the intrinsic features of the system under study: finite size, presence of the Coulomb interaction, lack of homogeneity, etc. Some ways of identifying liquid-gas phase transitions, directly from heavy ion collision data are discussed. Finally, a study aiming to identify an equilibrated stage in a dynamical multifragmentation path as provided by a transport code is presented.

I. INTRODUCTION

One may generally define multifragmentation as the break-up of any physical system into many "pieces". The above definition thus includes the break-up of various physical objects, *e.g.*, a porcelain plate, the sand grain formation or even a supernova explosion, etc. From a thermodynamical view, these phenomenas are interesting since they may correspond to a uniform population of the system's associated phase space and sometimes may be related to phase transitions.

Nuclear multifragmentation is obtainable in laboratories by violently colliding atomic nuclei. Due to the resemblance of the nucleon-nucleon interaction with the van der Waals forces, this phenomenon may be related to a liquid-gas phase transition [1]. Lots of theoretical and experimental studies have been performed trying to elucidate whether a liquid-gas phase transition is *really* taking place in nuclear matter.

Experimentally, first indication about a phase transition was reported in 1995 by the ALADIN group [2]. With that occasion, a plateau of the temperature versus excitation energy curve (*i.e.*, caloric curve) was identified at appx. 5 MeV temperature. Plateau-like regions in the caloric curves evaluated by various

statistical models like SMM [4], MMMC [3] and, more recently, MMM [5] where also reported. However, in order to have a rigorous proof about a phase transition one has to identify the thermodynamical constraints of the system under study. This is a complicated task from the experimental point of view since the initial, possibly equilibrated signal, is polluted by various phenomenas such as prefragment emission or subsequent secondary decays.

In laboratories one can only study *asymptotic* fragments sizes and kinematic distributions. These observables are to be compared with the results of various dynamical and statistical models. Good agreements between statistical calculations and experiments provide indications that a *statistically equilibrated* fragmenting source is at the origin of the experimentally obtained yields.

This raises two important questions: 1. Is statistical equilibrium *really* at the origin of the (experimentally) observed nuclear multifragmentation phenomena? Indeed, good agreements in the *asymptotic stage* between statistical models and data represent a *necessary* condition for equilibrium but not a *sufficient* one. 2. If a statistically equilibrated source does exist, then is there any way to get experimental information about a liquid-gas phase transition unaffected by the above-discussed polluting phenomenas?

One may basically divide the theories aiming to investigate this phenomenon into *dynamical* and *statistical* ones. From the dynamical models the most effective are the Landau Vlasov or the Quantum Molecular Dynamics ones. They mimic the evolution in time of the collision process. The statistical theories are based on the assumption that a statistically equilibrated stage, occurs in the dynamical path. Their common ingredient is equal probability between all fragmentation possibilities. As will be seen, these two classes of theories are complementary and may be used as and unitary tool for analyzing the system's thermodynamics.

There are further interesting questions related to multifragmentation which will be addressed in the present article: Which is the time in the system's dynamical evolution corresponding to statistical equilibrium? How does the statistically equilibrated stage "looks like"? *E.g.* are fragments already completely formed and separated or the statistical equilibrium rather corresponds to a prefragment stage scenario? Which is the volume of the system corresponding to the equilibrium stage? Which factors are influencing the phase transition or the nuclear phase diagram?

II. PREVIOUS STATISTICAL DEVELOPMENTS

Statistical ensembles are powerfull instruments for investigating the nuclear multifragmentation phenomenon. Due to the finite size of the nuclear systems, the microcanonical ensemble is the most adequate for studying such phenomenas.

However, due to the huge number of contributing configuration and due to the fact that such ensembles are not analytically tractable any attempt to perform direct computation is useless. One generally uses ensembles with fewer constraints (*e.g.* canonical or grandcanonical) numerically solvable or tries to make statistical simulations of the microcanonical ensemble (using standard Monte Carlo or Metropolis Monte Carlo methods) starting from the associated microcanonical weights. Two models trying to follow the microcanonical rules widely used indata analysis are the MMMC [3] and SMM [4] models. However, none of these models sharply follow the microcanonical ensemble. A more rigorous microcanonical development, however mostly schematic is due to Koonin and Randrup [6]. The Microcanonical Multifragmentation Model (MMM) [5] starts from the Koonin and Randrup concepts effectivelyadapting them to the complexity of the nuclear multifragmentation phenomenon. This model sharply simulates the microcanonical ensemble.

III. MICROCANONICAL MULTIFRAGMENTATION MODEL

The microcanonical multifragmentation model (MMM) used in the present study was proposed in Ref. [5] and was further refined and developed in Ref. [14]. The model simulates various stages of the multifragmentation phenomenon: the primary break-up stage which is considered statistically equilibrated and treated microcanonically; fragments' momentum generation with inclusion of collective radial expansion; Coulomb propagation, and the secondary emission stage.

A. BREAK-UP

This stage concerns the disassembly of a statistically equilibrated nuclear source (A, Z, E, V) (the mass number, the atomic number, the excitation energy and the freeze-out volume respectively). Equal probability between all configurations $C:\{A_i,\ Z_i,\ \varepsilon_i,\ \mathbf{r}_i,\ \mathbf{p}_i,\ \ i=1,\ldots,N\}$ (the mass number, the atomic number, the excitation energy, the position and the momentum of each fragment i of the configuration C, composed of N fragments) is assumed. Fragments are considered spherical, do not overlap each other and are placed into a spherical recipient of volume V. The system is subject to the following microcanonical constraints: $\sum_i A_i = A,\ \sum_i Z_i = Z,\ \sum_i \mathbf{p}_i = \mathbf{P},\ \sum_i \mathbf{r}_i \times \mathbf{p}_i = \mathbf{L},\ E$ – constant. The integration over fragment momenta can be analytically performed subject to the above mentioned constraints:

$$\int\prod_{i=1}^{N} \mathrm{d}\mathbf{p}_i\ \delta(H-E)\,\delta\left(\sum_i \mathbf{p}_i - \mathbf{P}\right)\delta\left(\sum_i \mathbf{r}_i \times \mathbf{p}_i - \mathbf{L}\right) =$$

$$= \frac{2\pi}{\Gamma\left(\frac{3}{2}(N-2)\right)}\left(\frac{\prod_i m_i}{\sum_i m_i}\right)^{3/2} \frac{1}{\sqrt{\det \mathbf{I}}}\left[2\pi\left(K - \frac{P^2}{2M} - \frac{1}{2}\mathbf{L}^T\mathbf{I}^{-1}\mathbf{L}\right)\right]^{\frac{3}{2}(N-2)-1} \quad (1)$$

Here $M = \sum_i m_i$, $\mathbf{I}$ is the inertial tensor of the system: $I_{\alpha\beta} = \sum_i m_i\left(r_i^2\delta_{\alpha\beta} - r_i^\alpha r_i^\beta\right)$ with α, β = 1, 2, 3, $\mathbf{L}^T\mathbf{I}^{-1}\mathbf{L} = \sum_{\alpha\beta=1}^{3} L_\alpha I_{\alpha\beta}^{-1} L_\beta$ and K is the kinetic energy of the system. The statistical weight of a configuration $C' : \{A_i,\ Z_i,\ \varepsilon_i,\ \mathbf{r}_i,\ i = 1, \ldots, N\}$ writes:

$$W_{C'} = \frac{1}{N!}\frac{2\pi}{\Gamma\left(\frac{3}{2}(N-2)\right)}\frac{1}{\sqrt{\det \mathbf{I}}}\left[\prod_i\left(\frac{\rho_i(\varepsilon_i)}{h^3}\right)\right]\left(\frac{\prod_i m_i}{\sum_i m_i}\right)^{3/2} \times$$

$$\times\left[2\pi\left(K - \frac{P^2}{2M} - \frac{1}{2}\mathbf{L}^T\mathbf{I}^{-1}\mathbf{L}\right)\right]^{\frac{3}{2}(N-2)-1} \delta\left(\sum_i A_i - A\right)\delta\left(\sum_i Z_i - Z\right)\times \quad (2)$$

$$\times\Theta(K)\,\delta\left(\sum_i \mathbf{p}_i - \mathbf{P}\right)\delta\left(\sum_i \mathbf{r}_i \times \mathbf{p}_i - \mathbf{L}\right)$$

One generally uses $\mathbf{P} = 0$ and $\mathbf{L} = 0$.

The weights $W_{C'}$ are further employed in a Metropolis-type simulation which allows the determination of the average value of any system observable.

Fragments with $A \leq 4$ are considered without excitation degrees of freedom except for the α particle for which the few levels larger than 20 MeV with G ≤ 3 MeV have been considered. These fragments are weighted in $W_{C'}$ with their energy levels degeneracies. Larger fragments carry internal excitation. For them, the following level density formula is included in the statistical weight of a configuration C':

$$\rho(\epsilon) = \frac{\sqrt{\pi}}{12\, a^{1/4}\epsilon^{5/4}} \exp(2\sqrt{a\epsilon}) \exp(-\epsilon/\tau) \quad (3)$$

with $a = 0.114A + 0.098A^{2/3}$ MeV^{-1}. τ is a free parameter. The factor $\exp(-\epsilon/\tau)$ was introduced to account for the dramatic decrease of the excited levels lifetime at high excitation energies but can also compensate the various model approximations (*e.g.* in reality fragments may be deformed).

B. GENERATION OF THE PRIMARY DECAY FRAGMENT MOMENTA

While integration over the fragments' momenta has been carried out in order to simplify the Metropolis simulation, to produce events similar to the

experimental ones on has to generate momenta for each given configuration C'. Each of these events are characterized by a kinetic energy K. Therefore, we have to deal with the following computational task: generate uniformly momenta for a system composed of N particles such that $\sum_i p_i^2/2m_i = K$, $\sum_i \mathbf{p}_i = 0$ and $\sum_i \mathbf{r}_i \times \mathbf{p}_i = \mathbf{L}$. This problem was solved in an elegant way in Ref. [9]. There, it is proved that the following generation gives the right sampling of the system momenta, in agreement with the above mentioned constraints: Pick a preliminary set of N particle momenta from a arbitrary canonical distribution, then eliminate the overall translational and rotational motion by making the transformation $\mathbf{p}_i \to \mathbf{p}_i - m_i(\mathbf{P}'/M + \boldsymbol{\omega}' \times \mathbf{r}_i)$ (where $\mathbf{P}' = \sum_i \mathbf{p}_i$ and $\boldsymbol{\omega}' = \sum_i \mathbf{r}_i \times \mathbf{p}_i \cdot \mathbf{I}^{-1}$), then spin the system such as to match the desired angular momentum $\mathbf{L}: \mathbf{p}_i \to \mathbf{p}_i + m_i\, \boldsymbol{\omega} \times \mathbf{r}_i)$ with $\boldsymbol{\omega} = \mathbf{L}^T \cdot \mathbf{I}^{-1}$ and finally, renormalize the momenta such as to match the available energy $K - \frac{1}{2}\boldsymbol{\omega} \cdot \mathbf{L}$.

C. RADIAL FLOW

After generating the fragment momenta corresponding to the primary decay, inclusion of nonequilibrium effects such as collective radial expansion (*flow*) can be easily superimposed. Here we use the following parametrization for the flow velocity of fragment i: $\mathbf{v}_f^i = \mathbf{v}_0\, (r_i/R)^{\alpha}$, with $\mathbf{v}_0 = v_0(\mathbf{r}_i/r_i)$ and α a real number defining the flow profile. After including the radial flow, the momentum of the ith fragment reads: $\mathbf{p}_i \to \mathbf{p}_i + m_i \mathbf{v}_f^i$.

D. COULOMB PROPAGATION

After break-up, hot primary fragments are supposed to suffer an expansive propagation under their mutual Coulomb interaction. This stage can be easily simulated by integrating the corresponding Newtonian equations of motion. Integration has been carried out up to 500 fm/c, when Coulomb interaction between fragments can be neglected.

E. SECONDARY DECAYS

Since primary fragments carry internal excitation, a secondary decay stage was introduced in Ref. [10]. Depending on the fragment excitation, secondary break-up processes or particle evaporation was considered. Since the above classification was rather arbitrary, here we resume to the second process, treated

using the standard Weisskopf evaporation scheme. As in [10], the range of the evaporated particles is considered up to $A = 16$. Evaporation events are simulated using standard Monte Carlo [10].

For each primary break-up event A, the steps B–E are performed. The resulted fragmentation events can be readily compared with experimental ones (with the preequilibrium particles removed).

IV. MMM RESULTS *VS.* EXPERIMENTAL DATA

The MMM model provides very good description of experimental data. This section will give an example in this direction by describing an attempt to simultaneously fit various fragment size and kinematic experimental distribution by means of MMM [14]. The experimental data concern the reactions Xe + Sn at 32 MeV/u and Gd+U at 36 MeV/u published by the INDRA collaboration in

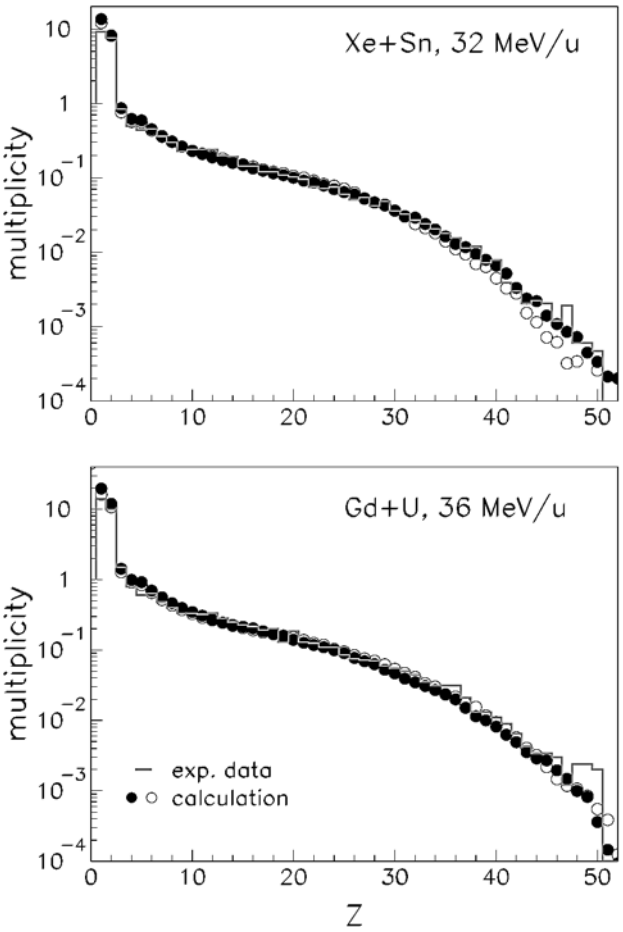

Fig. 1 – Charge distribution corresponding to the reactions Xe + Sn at 32 MeV/u and Gd + U at 36 MeV/u. The MMM results are compared with the experimental results of the INDRA collaboration.

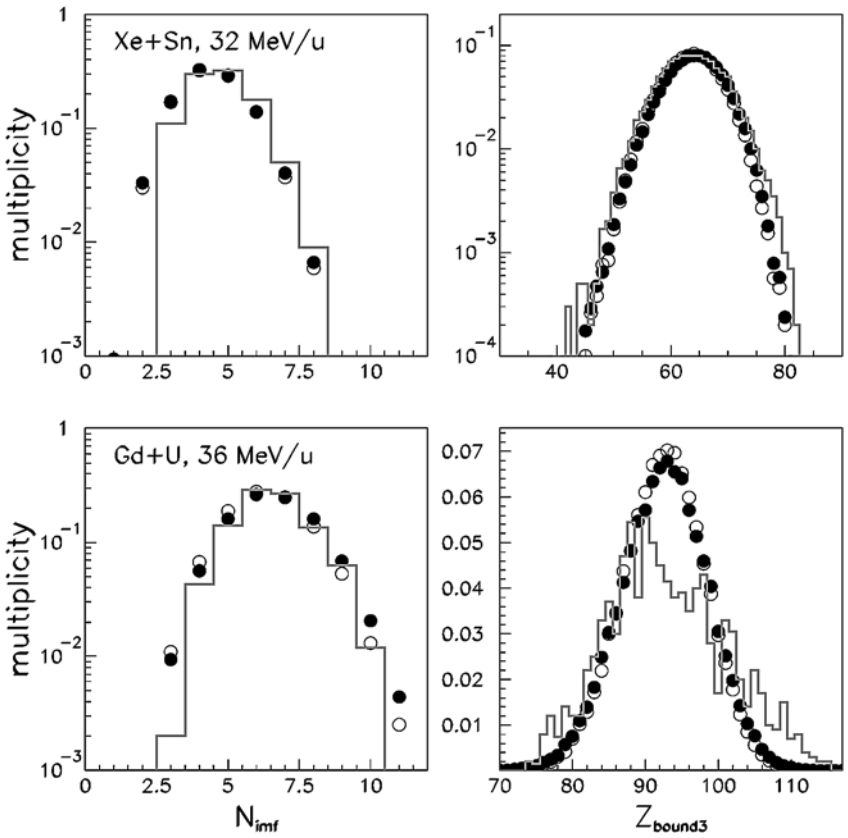

Fig. 2 – Intermediate mass fragments and *bound charge* multiplicities for the reactions Xe+Sn at 32 MeV/u and Gd+U at 36 MeV/u. The MMM results are compared with the experimental results of the INDRA collaboration.

Ref. [7, 8]. For these comparisons the parameter τ was fixed to an arbitrary value of 9 MeV and two different freeze-out hypotheses have been used.

Indeed, it is well known that various freeze-out assumptions induce differences in the statistical models' results. For reducing this uncertainty two "opposite" freeze-out scenarios have been employed:

1) The standard working hypothesis of the model: Fragments are idealized as hard spheres placed into a spherical freeze-out recipient; fragments are not allowed to overlap each other or the recipient wall. The generation of the fragments' positions is described in Ref [5].
2) The fragment hardcore interaction is switched off: An approximate integration over the fragments' positions is carried out by assuming as in Ref. [11] that each fragment (from a configuration composed of N fragments) is blocking the volume V_0N (V_0 is the volume of the nuclear system at normal density) for the rest of the fragments and for itself as well. The

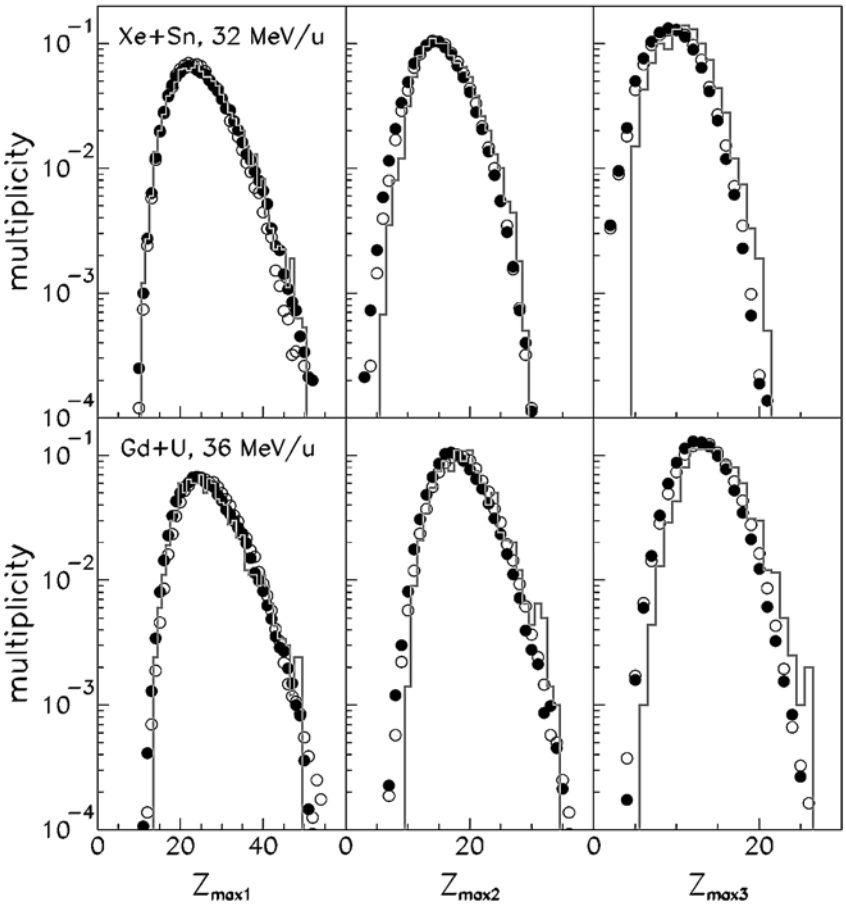

Fig. 3 – Multiplicities of largest, second largest and third largest fragments. MMM results are compared with the experimental results of the INDRA collaboration.

Coulomb energy is approximated by the Wigner Seitz formula, being therefore independent of the fragments' positions. For a N fragment partition the Wigner Seitz Coulomb interaction energy writes:

$$V_{WS} = \frac{3}{5}\left(Z^2/R - \sum_{i=1}^{N} Z_i^2/R_C^i \right) e^2 \tag{4}$$

where R is the radius of the freeze-out recipient and R_C^i is the radius of the Wigner Seitz cell corresponding to the fragment i, $R_C^i = r_0(nA_i)^{1/3}$ where $r_0 = 1.2$ fm, and $n = V/V_0$. The integration over the fragments' positions writes:

$$\int\prod_{i=1}^{N} \mathrm{d}\mathbf{r}_i \frac{1}{\sqrt{\det \mathbf{I}}} \prod_{j<i} \theta_{ij} \simeq V_{free} \int\prod_{i=1}^{N} \mathrm{d}\mathbf{r}_i \frac{1}{\sqrt{\det \mathbf{I}}} \tag{5}$$

with:

$$V_{free} = \prod_{i=1}^{N} \left(V - i\frac{V_0}{N} \right). \tag{6}$$

The factor $\prod_{j<i} \theta_{ij}$ from eq. (5) is just a formal expression of the fragment blocking constraint formulated before. Within this freeze-out hypothesis, fragment positions have to be generated into the spherical freeze-out volume, without any hardcore constraints just for evaluating $\det \mathbf{I}$ and the statistical weight of a configuration will get the extra factor V_{free}. Having the weights $W_{C'}$, the corresponding Metropolis simulation is straight forward [5].

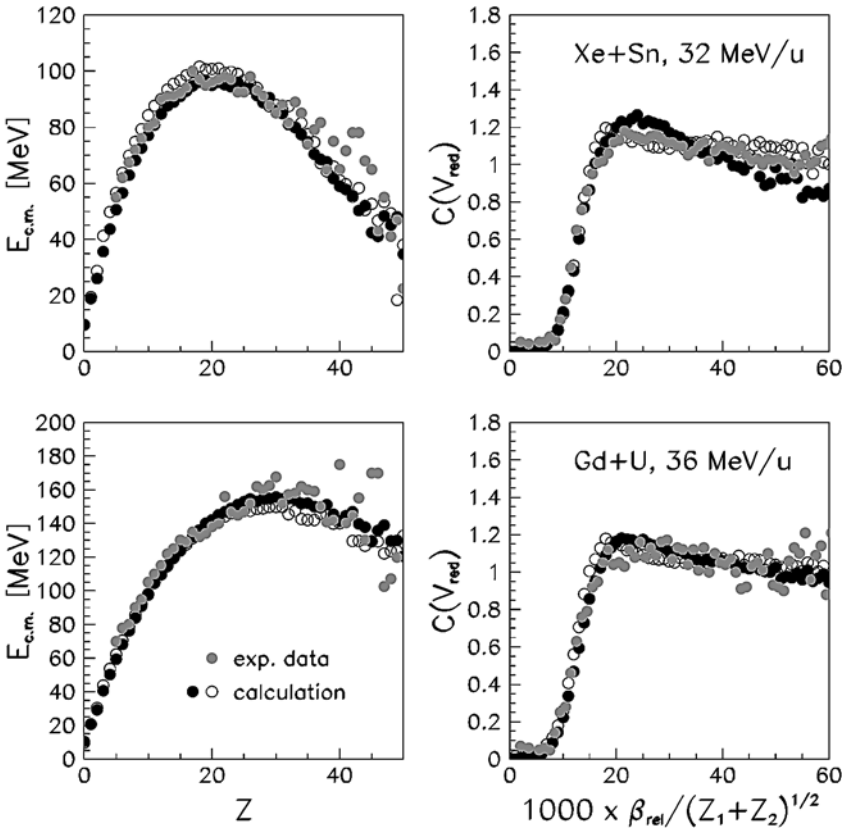

Fig. 4 – Kinetic energy distributions vs charge and velocity correlations (bottom) corresponding to the reactions Xe + Sn at 32 MeV/u and Gd + U at 36 MeV/u. MMM results are compared with the experimental results of the INDRA collaboration.

The results of this comparison are summarized in Figs. 1–4 (see Ref. [14] for more details). As can be seen, all fragments yields, velocity correlations and kinematic experimental distributions corresponding to both reactions are simultaneously reproduced in both freeze-out hypotheses. Some comments are in order: like all other direct comparisons with experimental data, these fits have been performed directly on the experimental asymptotic yields. The τ parameter was arbitrary fixed to a value of 9 MeV. More accurate analyzes should vary the parameter τ as well and should be performed in the primary decay stage. The last requirement is presently possible only by using the data of a transport mode. Such an analysis will be described in a subsequent section. Nonetheless, the enclosed results illustrate the excellent MMM capabilities for fitting the experimental data.

V. FIRST ORDER PHASE TRANSITION IN NUCLEAR MATTER?

Nuclear systems are *finite* and *electrically charged* – so *non-extensive*. As we know, thermodynamics has been designed for infinite extensive systems. One cannot make standard thermodynamics on nuclear system: one may rather speak about a "small systems thermodynamics".

For such systems, a good way to obtain information about a possible liquid-gas phase transition is to use the techniques commonly employed for the large systems. In this respect, the caloric curves at constant pressure, $T(E)|_P$ or the pressure versus volume curves at constant temperature, $P(V)|_T$ have to signal the presence of the phase transition. Temperature is simply deducible within MMM by evaluating $(\partial S/\partial E)^{-1}$ (where S is the entropy of the system) [15]. However as we aim the deduction of the isobars $T(E)|_P$ or the isotherms $P(V)|_T$ we will use the probability density of canonical ensembles in order to deduce these quantities.

The probability density for obtaining an event with total energy E and volume V within an isobaric canonical ensemble characterized by the parameters β (inverse of canonical temperature) and P (canonical pressure) writes:

$$\mathcal{P}(E,V)=\frac{W(E,V)\,e^{-\beta E-\beta PV}}{Z_{can}(\beta,P)}, \tag{7}$$

where $W(E, V)$ is the microcanonical density of states corresponding to a system characterized by the excitation energy E and the volume V, and $Z_{can}(\beta, P)$ is the partition function of the canonical ensemble at constant pressure: $Z_{can}(\beta,P)=\int\mathrm{d}E\int\mathrm{d}V\,W(E,V)\,e^{-\beta E-\beta PV}$. Then, the microcanonical entropy ($S=\ln W(E, V)$) can be written as:

$$S(E,V) = \ln \mathcal{P}(E,V) + \beta E + \beta PV + \ln Z_{can}(\beta, P). \tag{8}$$

The first three terms of the sum in eq. (8) can be regarded as a *relative* entropy of the system $(S_r(E,V) = S(E,V) - \ln Z_{can}(\beta, P))$. Furthermore, $\ln \mathcal{P}(E,V)$ can be regarded as a "cut" through the surface of the entropy $S(E, V)$ with the plane $\beta E + \beta PV + \ln Z_{can}(\beta, P)$. This implies that a double peaked structure of $\ln P(E, V)$ reflects a convex intruder in the entropy surface which is related to a first order phase transition. The microcanonical temperature (T_μ) and pressure (P_μ) can be evaluated from eq. (8) starting from their definitions ($T_\mu = (\partial S(E,V)/\partial E)^{-1}$, $P_\mu = T_\mu \partial S(E,V)/\partial V$):

$$\begin{aligned} T_\mu &= \left(\beta + \frac{\partial \ln P(E,T)}{\partial E} \right)^{-1}, \\ P_\mu &= T_\mu \left(\beta P + \frac{\partial \ln P(E,T)}{\partial V} \right). \end{aligned} \tag{9}$$

The above equations provide a nice solution for the problem of constructing the isobaric $T(E)$ curves or the isothermal $P(V)$ curves: 1. Simulate the canonical ensemble at constant pressure corresponding to the parameters β and P – this can be easily achieved within the present microcanonical model [5] by simply replacing the statistical weight corresponding to the configuration C, $W(C)$, by $W(C)\, e^{-\beta E - \beta PV}$ and letting both energy and volume to fluctuate. 2. Collect the corresponding probability distributions $P(E, V)$. 3. Evaluate the pair (T_μ, P_μ) for each point (E, V) for which the number of collected events is sufficiently large to acquire a good statistics. 4. Choose a path (in the (E, V) plane) of *constant* microcanonical pressure (equal to the canonical one P) or respectively of *constant* microcanonical temperature (equal to the canonical one $1/\beta$). A similar method was used in Ref. [17] for extracting microcanonical $T(E)$ curves from unidimensional canonical energy distributions within the Lattice Gas Model.

Using this method, isobaric caloric curves corresponding to various pressures were constructed for the source (200, 82) (*i.e.*, A = 200 and Z = 82) in two situations. In the first case Coulomb energy was present both in the fragments' liquid-drop binding energies and interfragment interaction. As it can be observed in Fig. 5 (left) all the caloric curves manifest a monotonic increase regardless the considered pressure. Even smaller pressures than those corresponding to the curves from Fig. 1 were tested with the same result. One may conclude that there is no phase transition taking place in this system. In the second situation, the Coulomb energy was suppressed from both the liquid-drop binding energies of the fragments and from the interfragment interaction. This

time all isobaric caloric curves backbend which is an indication of the occurrence of a first order phase transition (see Fig. 5 – right). In the lower part of Fig. 5 the quantity $\ln \mathcal{P}(E,V)$ is represented for the canonical pressure $P = 2.5 \cdot 10^{-2}$ MeV/fm^3 in both "with" and "without Coulomb" cases. The canonical temperature 1/β was chosen in each case such as to provide a distribution of events covering the plateau-like region in the "with Coulomb" case and the backbending region in the "without Coulomb" case. While in the "with Coulomb" case the distribution has a single peak reflecting the absence of any phase transition, in the "without Coulomb" case a double peaked structure indicates the presence of a first-order phase transition. In this case the peak corresponding to the lower energies can be associated to the liquid phase while the one corresponding to the higher energies can be attributed to the gas phase. If

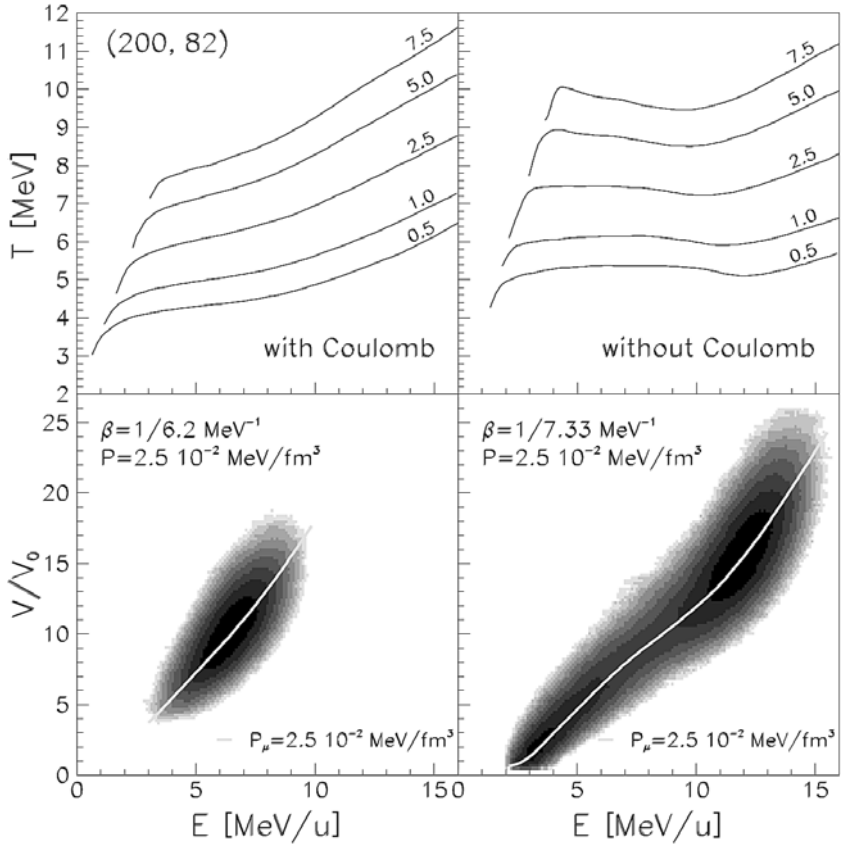

Fig. 5 – Isobaric caloric curves (top); Probability distributions of isobaric canonical ensembles (bottom). Calculation were performed with MMM for a nuclear source with A = 200 the case in which Coulomb interaction in present (left column) and in the case in which Coulomb interaction is absent (right column).

the canonical parameters (β and P) are chosen such as the peaks are of equal height, the interval between the peaks sharply defines the coexistence region. The path of constant pressure ($P_\mu = P$) will *necessarily* pass through the maxima of the distributions (see Fig. 5) implying that the isobaric path provides a natural order parameter even for small systems.

The same analysis is further performed for a smaller, charged system: the (50,23) nucleus. The result is presented in Fig. 6. It can be noticed that for pressures smaller than 10^{-2} MeV/fm^3 slight backbendings are present.

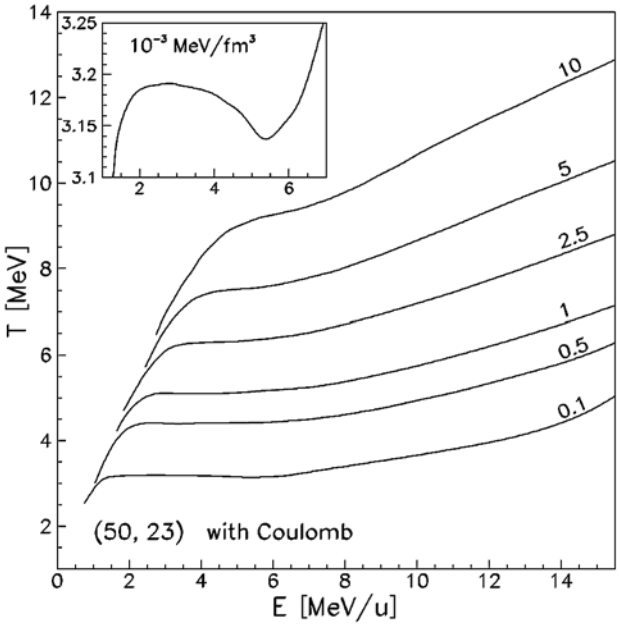

Fig. 6 – Isobaric caloric curves for a nuclear source with A = 50 calculated with MMM. Coulomb interaction is present.

Two conclusions may be drawn from this analysis: 1) *The MMM model exhibits a first order phase transition.* 2) *Coulomb interaction acts towards lowering the system's critical point.* In other words, Coulomb field may forbid the phase transition when it is too strong (*e.g.* large nuclei like A = 200 and Z = 82 – see Fig. 5). For smaller nuclei (*e.g.* A = 50, Z = 23), where the Coulomb amount is smaller, the 1st order phase transition survives (see Fig. 6). See Ref. [16] for more details.

VI. WAYS TO IDENTIFY LIQUID-GAS PHASE TRANSITIONS (IN EXPERIMENTAL DATA)

While phase transition was predicted within various models, including MMM, from the experimental point of view so far things are inconclusive. The

reasons are related to both the inherent difficulties of backtracking the freeze-out stage and the lack of any rigorous method allowing the determination of a liquid-gas phase transition when it exists in experimental data.

Some years ago the general impression was that the experimental nuclear caloric curve could decide on the existence of a first order phase transition. Grandcanonical isotopic thermometers were extensively used. Appart from the weaknesses of each "thermometers" tested with that occasion, one fundamental barrier is preventing unambiguous identification of a first order phase transition from the experimentally obtained caloric curve: The experimentally generated (microcanonical) systems follow an *unknown* path in the excitation energy (E)-freeze-out volume (V) plane. *Even* if the experimental path intersects the coexistence region the phase transition may remain unrevealed in the caloric curve. For overcoming that situation it was proposed that the heat capacity being a quantity *independent* on the experimental path but depending on the *local* freeze-out constrain could give information concerning the occurrence of the transition [19]. More precisely, if the experimental path is crossing the system's spinodal region of the this has to be signaled by a negative value of the heat capacity. An approximate analytical heat capacity formula was proposed and subsequently tested on the experimental data obtained of the MULTICS-MINIBALL collaboration. With that occasion, negative branches of the heat capacity curves were identified [20].

In the present section we will describe an exact, microcanonical way to calculate the heat capacity [18] which should effectively reveal phase transitions where present in data.

A. MICROCANONICAL HEAT CAPACITY

Function of the desired conservation restriction ($\mathcal{R}$) level (n) one can express the statistical weight of a configuration $C' : \{A_i,\ Z_i,\ \varepsilon_i,\ \mathbf{r}_i,\ i = 1,\ldots,N\}$ (this weight was first expressed in Section I):

$$W_{C'} \propto I_p = \int\!\!\prod_{i=1}^{N} \mathrm{d}\mathbf{p}_i\, R(n) = \frac{2\pi \prod_i m_i^{3/2}}{\Gamma\left(\frac{3}{2}(N-n)\right)} f(n) \left(2\pi K\right)^{\frac{3}{2}(N-n)-1}, \tag{10}$$

with $n = 0,\ 1,\ 2;\quad \mathcal{R}(0) = \delta\left(H - E\right),\quad \mathcal{R}(1) = \mathcal{R}(0)\,\delta\left(\sum_i \mathbf{p}_i\right),\quad \mathcal{R}(2) = \mathcal{R}(1)\cdot$ $\cdot\delta\left(\sum_i \mathbf{r}_i \times \mathbf{p}_i\right);\ \ f(0) = 1,\ \ f(1) = 1/\left(\sum_i m_i\right)^{3/2}\right)$ and $f(2) = f(1)/\sqrt{\det \mathbf{I}}$, where $\mathbf{I}$ is the inertial tensor of the system. Here H denotes the system's Hamiltonian: $H = \sum_i p_i^2/(2m_i) + \sum_{i<j} V_{ij} + \sum_i \epsilon_i - \sum_i B_i$ and $K = E - \sum_{i<j} V_{ij} - \sum_i \epsilon_i +$

$+\sum_i B_i$ (V_{ij} is the Coulomb interaction between fragments *i* and *j*; ϵ_i and B_i are respectively the internal excitation and the binding energy of fragment *i*). The microcanonical density of states corresponding to a total energy of the system *E* can be expressed:

$$W(E) = \sum_{C'} W_{C'} \tag{11}$$

where

$$W_{C'} = \frac{1}{N!}\left(\prod_{i=1}^{N} \frac{\rho_i(\epsilon_i)}{h^3}\right) F(\mathcal{P}) f(n) \left[2\pi(E-\mathcal{E})\right]^{\frac{3}{2}(N-n)-1} \tag{12}$$

and

$$\sum_{C'}() \equiv \oint \mathrm{d}\mathcal{E}() \equiv \sum_{N=1}^{A} \prod_{i=1}^{N} \left(\sum_{A_i,Z_i} \int \mathrm{d}\mathbf{r}_i \int \mathrm{d}\epsilon_i \right)() \tag{13}$$

Here $F(\mathcal{P})$ is the factor in front of $f(n)$ from eq. (10), ($\mathcal{P}$ is a generic notation for fragment partition) and $\mathcal{E} \equiv \sum_{i<j} V_{ij} + \sum_i \epsilon_i - \sum_i B_i$.. The expression (13) is formal. Then, eq. (11) may be rewritten as:

$$W(E) = \oint \mathrm{d}\mathcal{E} \mathcal{F}(C') \left(E-\mathcal{E}\right)^{\frac{3}{2}(N-n)-1}. \tag{14}$$

The microcanonical temperature writes $T^{-1} = \partial S/\partial E$ with $S = \ln W(E)$. Which means:

$$T^{-1} = \frac{1}{W(E)} \frac{\partial W(E)}{\partial E} \tag{15}$$

If the limits of the integral over $\mathcal{E}$ are *not* depending on *E*, then one can make the derivative versus *E inside* the integral from eq. (14):

$$T^{-1} = \frac{1}{W(E)} \sum_{C'} W_{C'} \left(\frac{\frac{3}{2}(N-n)-1}{E-\mathcal{E}} \right) = \left\langle \frac{\frac{3}{2}(N-n)-1}{K} \right\rangle, \tag{16}$$

where we used the identity: $K = E - \mathcal{E}$ and the notation $\langle\ \rangle$ for the average over the ensemble's states. By definition, the heat capacity of the system is: $C^{-1} = -T^2\left(\partial^2 S/\partial E^2\right)$. Then, one obtains:

$$C^{-1} = 1 - T^2 \frac{1}{W(E)} \frac{\partial^2 W(E)}{\partial E^2}, \tag{17}$$

implying:

$$C^{-1}=1-T^2\left\langle\frac{\left[\frac{3}{2}(N-n)-1\right]\left[\frac{3}{2}(N-n)-2\right]}{K^2}\right\rangle. \tag{18}$$

Alternatively, one can evaluate the second order derivative of the system's entropy versus E:

$$\frac{\partial^2 S}{\partial E^2}=\left\langle\frac{\left[\frac{3}{2}(N-n)-1\right]\left[\frac{3}{2}(N-n)-2\right]}{K^2}\right\rangle-\left\langle\frac{\frac{3}{2}(N-n)-1}{K}\right\rangle^2. \tag{19}$$

In these terms, the spinodal region will coincide with the region with positive values of the above quantity. The microcanonical formulas given by eqs. (16), (18) and (19) are *universally* applicable to *any* system for which the "external" degrees of freedom can be treated classically irrespective to other specificity of the system. Indeed, the integral over the momenta variables (with the various possible conservation options) given in eq. (10), from which the microcanonical T, C and $\partial^2 S/\partial E^2$ formulas were further deduced is valid for any classical N particle system. This is the case of nuclear multifragmentation as well: it is widely accepted that, since at freeze-out the system is rather dilute, a classical treatment of the fragments' motion is appropriate. These features make eqs. (16), (18) and (19) suitable to be applied for experimental data: they are *independent* on specific model assumptions (*i.e.* freeze-out hypothesis, internal excitation treatment – level density, interfragment interactions, etc.), and moreover, they only depend on two parameters (K and N) which have to be estimated for the freeze-out stage.

B. TESTING THE HEAT CAPACITY FORMULAS

In the present Section we present some examples of the microcanonical heat capacity formulas functioning on different cases. To this aim, caloric curve and heat capacity curves are calculated by deriving the probability distributions of canonical ensemble as shown in Section III. These curves will be compared with the ones deduced using the microcanonical formulas. Calculations are performed with both freeze-out hypotheses of the model ((1) and (2) – see Section I), for two different freeze-out constraints: constant λ and constant volume, for the case in which the Coulomb interaction is present and the one in which it is switched off. (The "constant λ" constraint corresponds to a fluctuating volume, *i.e.* the microcanonical weights can be written as $W_{C'}\exp(-\lambda V)$). The considered conservation "level" is $n = 2$, *i.e.* the total energy, the momentum and

the angular momentum are conserved quantities. Results corresponding to the cases: (50, 23) nucleus with constant $\lambda = 5 \cdot 10^{-4}$ fm^{-3} with Coulomb interaction included, freeze-out hypothesis (2), (200, 82), $\lambda = 3 \cdot 10^{-3}$ fm^{-3}, without Coulomb interaction, freeze-out hypothesis (2) and the same nucleus with Coulomb interaction included, but a constant volume constraint: $V = 10V_0$, freeze-out hypothesis (1) are presented in Fig. 7 (first, middle and third column respectively). In the first two cases, backbendings of the caloric curves reflected in negative branches of the heat capacity curves and positive regions in the second order derivative of the entropy versus E – all related with a first order phase transition can be observed. In the third case (constant volume constraint) the caloric curve has a monotonic increase with a "plateau-like" region (where the curve slope is smaller, but positive) which is reflected in a positive C (with a

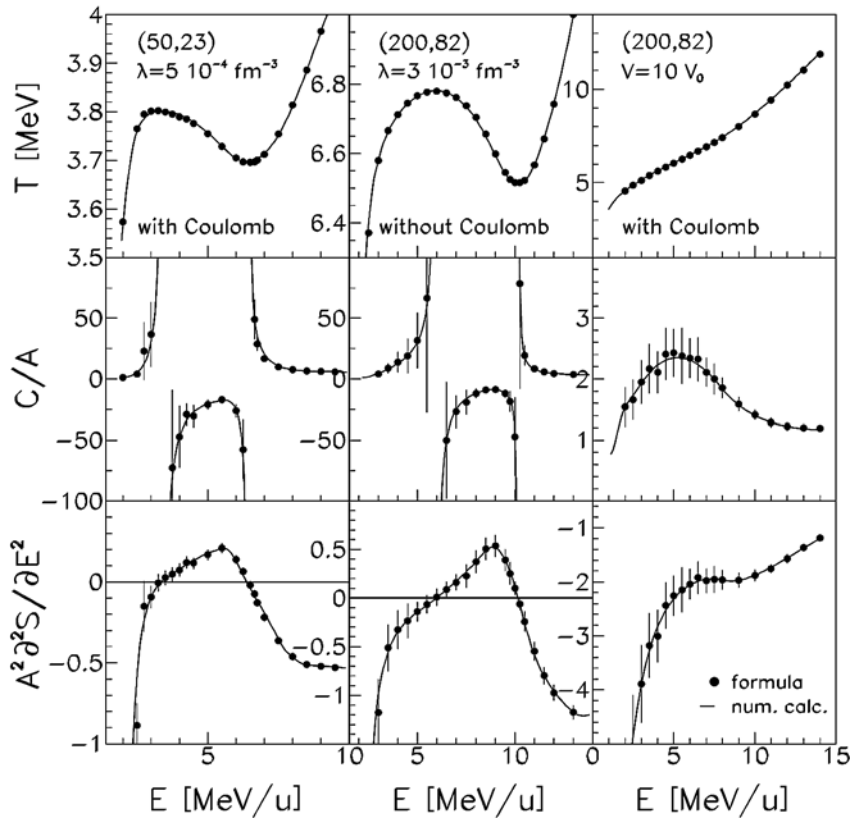

Fig. 7 – Comparison between the results of the microcanonical formulas (for temperature, heat capacity and second order derivative of the entropy) and the corresponding curves deduced from the probability distributions of a canonical ensemble with a given freeze-out constraint (*i.e.*, constant volume or constant λ). Each column correspond to the case labeled on it.

peak in the plateau-like region) and a negative $\partial^2 S/\partial E^2$. A very good agreement between the curves calculated using the probability distribution of a canonical ensemble and the points evaluated by means of the microcanonical formulas is to be noticed. The calculated microcanonical heat capacity and second derivative of the entropy versus excitation energy points are clearly revealing the spinodal region. Note that while the calculated heat capacity points have large error bars near the border of the spinodal region, $\partial^2 S/\partial E^2$ has small error bars even in the border region – *thus being a more robust quantity for identifying the spinodal region*.

C. EXTENSION OF THE MICROCANONICAL FORMULAS TO THE CASE OF FEWER FRAGMENTS

In practice it is difficult to experimentally get complete information about the freeze-out stage. Let us assume that only a number N_1 ($< N$) of fragments corresponding to a given event are experimentally detected. Is it still possible to evaluate the heat capacity? Turning back to eq. (10), for highest conservation level ($n = 2$) we can write:

$$\begin{aligned} I_p &= \int\prod_{i=1}^{N} \mathrm{d}\mathbf{p}_i\, \delta\left(\sum_i \frac{p_i^2}{2m_i} - K\right)\delta\left(\sum_i \mathbf{p}_i\right)\delta\left(\sum_i \mathbf{r}_i \times \mathbf{p}_i\right) = \\ &= \int \prod_{i=N_1+1}^{N} \mathrm{d}\mathbf{p}_i \int\prod_{i=1}^{N_1} \mathrm{d}\mathbf{p}_i\, \delta\left(\sum_{i=1}^{N_1} \frac{p_i^2}{2m_i} - K_1\right)\delta\left(\sum_{i=1}^{N_1} \mathbf{p}_i - \mathbf{P}_1\right)\delta\left(\sum_{i=1}^{N_1} \mathbf{r}_i \times \mathbf{p}_i - \mathbf{L}_1\right), \end{aligned} \tag{20}$$

where $K_1 = E - \mathcal{E} - \sum_{i=N_1+1}^{N} p_i^2/(2m_i)$, $\mathbf{P}_1 = -\sum_{i=N_1+1}^{N} \mathbf{p}_i = \sum_{i=1}^{N_1} \mathbf{p}_i$ and $\mathbf{L}_1 = -\sum_{i=N_1+1}^{N} \mathbf{r}_i \times \mathbf{p}_i = \sum_{i=1}^{N_1} \mathbf{r}_i \times \mathbf{p}_i$. The integration over the momenta of the first N_1 fragments is further performed:

$$\begin{aligned} I_p \propto \int \prod_{i=N_1+1}^{N} \mathrm{d}\mathbf{p}_i \left(K_1 - \frac{\mathbf{P}_1^2}{2M_1} - \frac{1}{2}\mathbf{L}_1{}^T\mathbf{I}_1^{-1}\mathbf{L}_1\right)^{\frac{3}{2}(N-2)-1} \times \\ \times\theta\left(K_1 - \frac{\mathbf{P}_1^2}{2M_1} - \frac{1}{2}\mathbf{L}_1{}^T\mathbf{I}_1^{-1}\mathbf{L}_1\right) \end{aligned} \tag{21}$$

where $\mathbf{I}_1$ is the inertial tensor corresponding to the first N_1 fragments at freeze-out, $M_1 \equiv \sum_{i=1}^{N_1} m_i$ and θ stands for the step function. One can further deduce the thermodynamical quantities as before. For the general case (*i.e.* a generic "level" of conservation n) one obtains:

$$T^{-1} = \left[\frac{3}{2}(N_1 - n) - 1\right]\left\langle\frac{1}{K_2}\right\rangle, \tag{22}$$

$$C^{-1} = 1 - T^2\left[\frac{3}{2}(N_1 - n) - 1\right]\left[\frac{3}{2}(N_1 - n) - 2\right]\left\langle\frac{1}{K_2^2}\right\rangle, \tag{23}$$

$$\frac{\partial^2 S}{\partial E^2} = \left[\frac{3}{2}(N_1 - n) - 1\right]\left[\frac{3}{2}(N_1 - n) - 2\right]\left\langle\frac{1}{K_2^2}\right\rangle - \left[\frac{3}{2}(N_1 - n) - 1\right]^2\left\langle\frac{1}{K_2}\right\rangle^2, \tag{24}$$

where $K_2 = K_1 - \mathcal{K}(n)$ with $\mathcal{K}(0) = 0$, $\mathcal{K}(1) = \mathbf{P}_1^2/(2M_1)$ and $\mathcal{K}(2) = \mathcal{K}(1) + {}$ $+ \mathbf{L}_1{}^T\mathbf{I}_1^{-1}\mathbf{L}_1/2$. The advantage of the above formulas is obvious: they only depend on one parameter (K_2) and, more importantly, they can be used for getting information about the liquid-gas phase transition even when one has *incomplete* information about the fragmentation events.

Of course, the success of any analysis involving these formulas depend on the accuracy of backtracking the information about the primary fragments from the experimentally detected asymptotic events.

VII. SEARCHING FOR THE EQUILIBRATED FREEZE-OUT IN A DYNAMICAL MULTIFRAGMENTATION PATH

Good agreements between various observables related to the asymptotically resulted fragments and various statistical models [3, 4, 6] indicated over the time that a huge part of the available phase space is uniformly populated during the fragmentation process and a statistically equilibrated nuclear source could stay at the origin of the experimentally observed nuclear multifragmentation data.

The source size, its excitation energy and its volume of the *assumed* source are quantities which are usually *indirectly* evaluated by comparisons between experimental data and statistical multifragmentation model predictions. The comparison process is complicated by the presence of several effects, such as pre-equilibrium particle emission, collective radial expansion, Coulomb propagation of the break-up primary fragments, secondary particle emissions.

However, the agreement at the level of asymptotic yields is only a *necessary* condition for equilibrium: One has to have *direct* access to the freeze-out events in order to *unambiguously* decide on the existence of a *statistically equilibrated stage*, and, if it does exists, to find its location in space and time. Presently, such an analysis is not possible on experimental data. An elegant solution is to perform a statistical analysis on a dynamical multifragmentation path of a transport model.

This kind of analysis makes the object of the present Section: The dynamical path of a stochastic mean field (SMF) approach [23] will be analyzed via the MMM model [5] in order to identify a possible equilibrated stage (see Ref. [24]). [5, 14].

A. STATISTICAL ANALYSIS ON THE DYNAMICAL PATH

We use the stochastic mean-field approach introduced in ref. [25]. According to this model, the fragmentation process is dominated by the growth of volume (spinodal) and surface instabilities encountered during the expansion phase of the considered excited systems. The dynamical evolution of the system is described in terms of the one-body distribution function (mean-field description), however this function experiences a stochastic evolution, in response to the action of the fluctuation term. The amplitude of the stochastic term incorporated in the treatment is determined by the degree of thermal agitation present in the system. Therefore, fluctuations provide the seeds of the formation of fragments, whose characteristics are related to the properties of the most unstable collective modes [26]. In SMF [25] fluctuations are implemented only in **r** space. Within the assumption of local thermal equilibrium, the kinetic fluctuations typical of a Fermi gas are projected on density fluctuations. Then, fluctuations are propagated by the unstable mean-field, leading to the disassembly of the system.

Using MMM we investigate whether along the dynamical path given by the stochastic mean-field approach as a result of the reaction ^{129}Xe+^{119}Sn at 32 MeV/u a distinct, statistically equilibrated stage exists. According to the dynamical simulations performed in Ref. [23], it is observed that, after the initial collisional shock, the system expands towards low densities entering the unstable region of the nuclear matter phase diagram (after about 100 fm/c from the beginning of the reaction). Then fragments are formed through spinodal decomposition. The dynamical freeze-out time is defined as the time when the fragment formation process is over, *i.e.* average fragment multiplicities and distributions do not evolve anylonger. For the reaction considered this time is 240 fm/c.

For washing-up pre-equilibrium effects that appear in the dynamical simulation, only intermediate mass fragments (IMF) (fragments with $Z \geq 3$) are considered for all comparisons between MMM and SMF. Due to the large Coulomb repulsion among primary fragments it is natural to assume that the largest deviation from the dynamical freeze-out to the statistical one concerns the volume. Therefore, the basic hypothesis of the present analysis is that while from the *statistically equilibrated freeze-out* to the *dynamical freeze-out* volume may change, all other source parameters be roughly conserved. For this reason, we will fit the fragment size distributions and their internal excitation energy but *not* the volume. The best fit can be found by minimizing the following error function:

$$Err = \left\{ 3\left[f(\langle A_{bound} \rangle) + f(\langle Z_{bound} \rangle) \right] + \left[\sum_{N_{IMF}} f[\langle \mathrm{d}N/\mathrm{d}N_{IMF} \rangle] / \sum_{N_{IMF}} 1 \right] + \right.$$
$$\left. + f\left(\langle \varepsilon_{IMF} \rangle\right) + \sum_{i=1}^{3} f\left(\langle Z_{\max i} \rangle\right)/3 \right\} /9 \qquad (25)$$

where $\langle \cdot \rangle$ stands for average, A_{bound} and Z_{bound} are the bound mass and charge (sum of the mass number and, respectively, atomic number of all IMF's from a

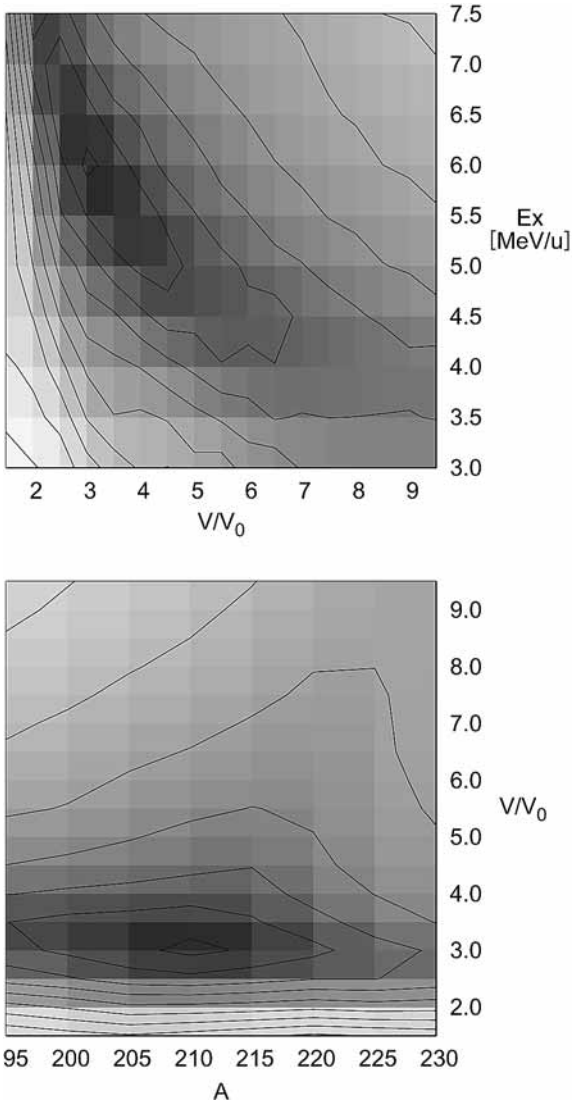

Fig. 8 – Contour plots of the error function *Err* [see eq. (1)]: in the (V/V_0, E) plane corresponding to $A = 210$ (upper panel); in the (A, V/V_0) plane corresponding to $E = 5.7$ MeV/u (lower panel). Darker regions correspond to smaller *Err*; units arerelative.

given event), N_{IMF} is the number of IMF's, ϵ_{IMF} is the excitation energy of one (IMF) fragment and $Z_{\max i}$ with $i = 1, 2, 3$ are the largest, second largest and third largest charge from one fragmentation event. Further, $f(x) = \left|2(x_s - x_d)/(x_s + x_d)\right|$, where the indexes s and d stand for "statistic" and "dynamic" and $|x|$ is the absolute value of x. MMM parameters A, E, V and τ are varied in wide ranges thus constructing a four-dimensional grid. The ranges are A : [195, 230], E : [3, 7.5] MeV/u, V/V_0 : [1.5, 9.5], τ = 12, 16, ∞ MeV.

B. RESULTS

An absolute minimum of the error function, *Err*, was found at $A = 210$, $Z = 87$, $V/V_0 = 3.4$, $E = 5.7$ MeV/u, $\tau = \infty$. Cuts in *Err* corresponding to $A = 210$

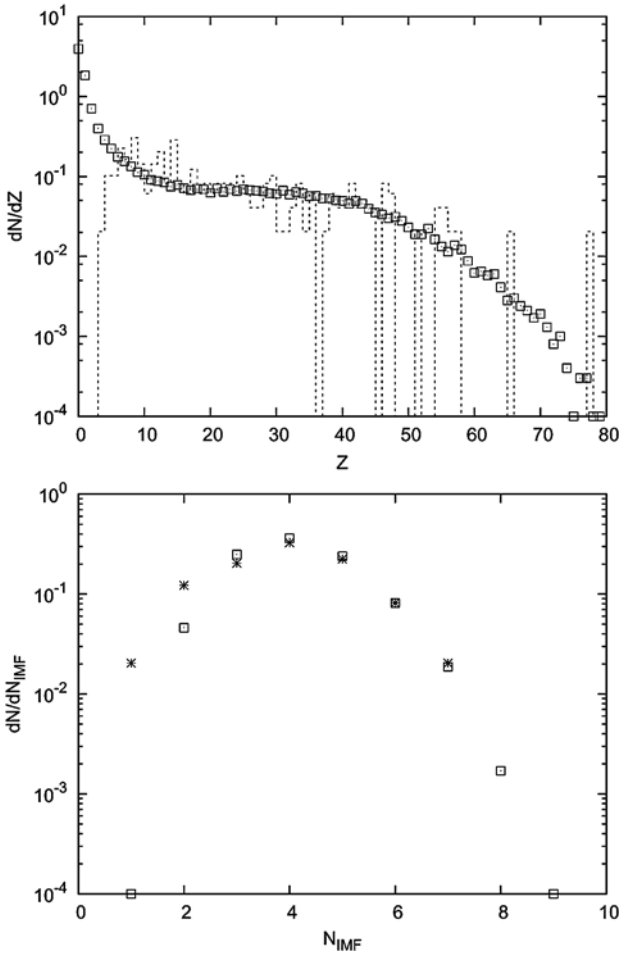

Fig. 9 – Dynamical charge (upper panel) and number of IMF distributions (lower panel) in comparisons with the statistical ones. Statistical results are represented by open squares; histogram (upper panel) and stars (lower panel) corespond to the dynamical ones.

and $E = 5.7$ MeV/u are represented in the upper part and respectively the lower part of Fig. 8. The statistical source corresponding to the minimum value of *Err* yields the following results: $\langle A_{bound} \rangle = 199.03$, $\langle Z_{bound} \rangle = 83.74$, $\langle \epsilon_{IMF} \rangle =$ $= 4.21$ MeV/u, $\langle Z_{\max 1} \rangle = 42.34$, $\langle Z_{\max 2} \rangle = 24.35$, $\langle Z_{\max 3} \rangle = 11.4$. These are to be compared with the corresponding *dynamical* results: $\langle A_{bound} \rangle = 199$, $\langle Z_{bound} \rangle =$ $= 84$, $\langle \epsilon_{IMF} \rangle = 4.3$ MeV/u, $\langle Z_{\max 1} \rangle = 41.95$, $\langle Z_{\max 2} \rangle = 22.5$, $\langle Z_{\max 3} \rangle = 13.3$. Note the excellent agreement for all considered observables, proving the very good quality of the fit. This can be also observed in Fig. 9 where the *dynamical* Z and N_{IMF} distributions fit perfectly the MMM ones. At this stage the question still remains: *even if fragment size distributions and excitation energies of the fragments are very well reproduced, do the dynamically formed fragments come from an equilibrated source with freeze-out volume* $V = 3.4V_0$, *as predicted by MMM?*

C. CHECKING THE PHYSICAL CONSISTENCY OF THE RESULTS

Within the present work the freeze-out volume V represents the volume of the smallest sphere *totally* including all fragments. We denote by $\widetilde{V}$ the volume of the smallest sphere *totally* including all fragments *and* with the center located in the center of mass of the system. Obviously, $\widetilde{V} > V$. The "dynamical" events have $\langle (\widetilde{V}/V_0)_{IMF} \rangle = 9.08$; the statistical ones have $\langle (\widetilde{V}/V_0)_{IMF} \rangle = 4.93$ (the *IMF* index indicates that we refer to the volume occupied by IMF fragments). According to this result, equilibration occurred at an earlier time compared to the time corresponding to the "dynamical freeze-out". One can simply test this hypothesis: one can propagate the fragments in their mutual Coulomb field from the freeze-out positioning as generated by MMM up to $(\widetilde{V}/V_0)_{IMF} = 9.08$ (*i.e.* the value corresponding to the "dynamical" events) and then compare "dynamical" and "statistical" fragment kinetic energies and positions. The best description of the dynamical results is obtained for a radial collective flow equal to zero. The comparison is presented in Fig. 10: the fragment average kinetic energies versus charge is represented in Fig. 10, upper panel; the radial distribution of the fragment with largest, second largest and third largest charge is represented in Fig. 10, lower panel. The time of the Coulomb propagation is around 100 fm/c. A surprisingly good agreement is observed between "dynamical" and "statistical" data for both observables indicating the physical consistency of the obtained result. This is an indication that the dynamical configurations could originate from an earlier *equilibrated* freeze-out ($t \approx 140$ fm/c), where fragments are located within a sphere (with the center in the center of mass of the system) of volume $\langle (\widetilde{V}/V_0)_{IMF} \rangle = 4.93$ and the collective flow is zero.

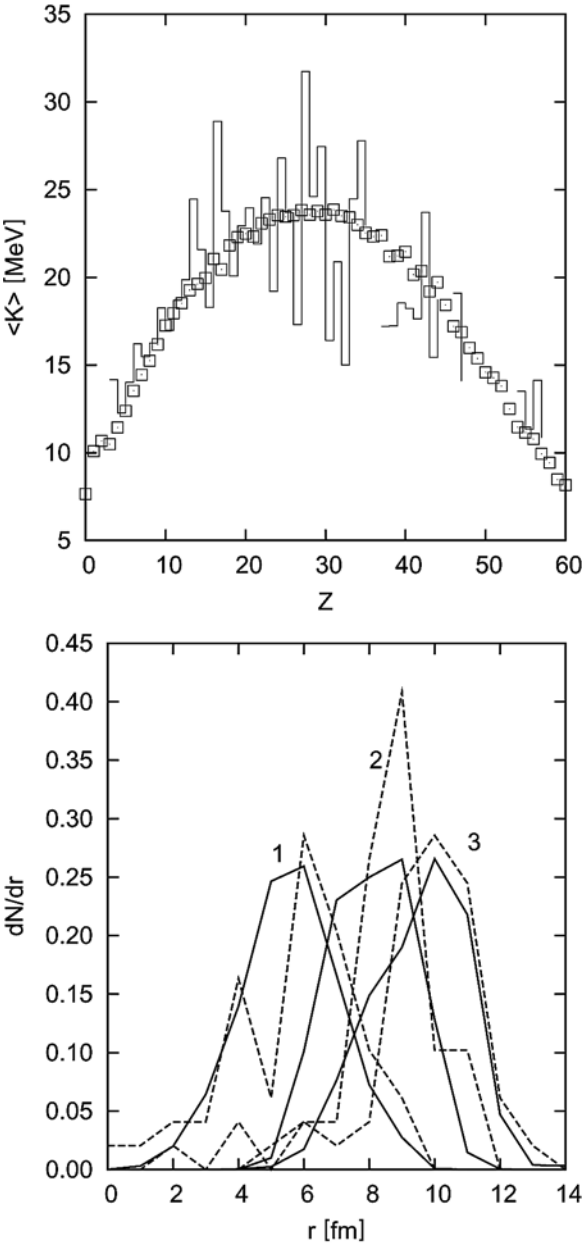

Fig. 10 – Upper panel: "statistical" (open squares) and "dynamical" (histogram) fragment average kinetic energy versus charge. Lower panel: "statistical" (solid lines) and "dynamical" (dashed lines) radial distribution of fragments with largest (peak "1"), second largest (peak "2") and third largest (peak "3") charge in one fragmentation event. The plot corresponds to $\left\langle (\widetilde{V}/V_0)_{IMF} \right\rangle = 9.08$.

In order to fully prove the physical consistency of our findings, we check what "happens" in the dynamical calculation at 140 fm/c. At that time the leading unstable modes are already well established and some pre-fragments, in strong interaction with the rest of the system, can be recognized [27]. These compounds are smaller respective to the final fragments and are surrounded by

nuclear matter at smaller density (nuclear "fog") which will eventually condensate on the pre-fragments increasing their size. In Fig. 11 (upper panel) we show the time evolution of the multiplicity of fragments and pre-fragments. The latter are identified as high density bumps, *i.e.* confined regions with density higher than the average. While the number of IMF's ends its variation at around 240 fm/c, remarkably the time evolution of the number of pre-fragments saturates at around 140 fm/c. This is precisely the *equilibration time* deduced with the above-described method. In Fig. 11 (lower panel) we show the behavior of the collective velocity, as obtained in the dynamical calculations at t = 140 fm/c, as a function of the distance from the center of mass of the system. One can observe that in the spatial region occupied by the prefragments (*i.e.* higher nuclear matter density, see the radial density profile on the same figure) the collective velocity is close to zero, which agrees with the MMM findings (see Fig. 10). And finally, on the same figure one can observe that the excitation energy of the fragmenting source, evaluated in the region occupied by pre-fragments, is rather constant as a function of the position and moreover is quite close to the excitation energy of the final fragments, meaning that at t = 140 fm/c the system is in thermal equilibrium.

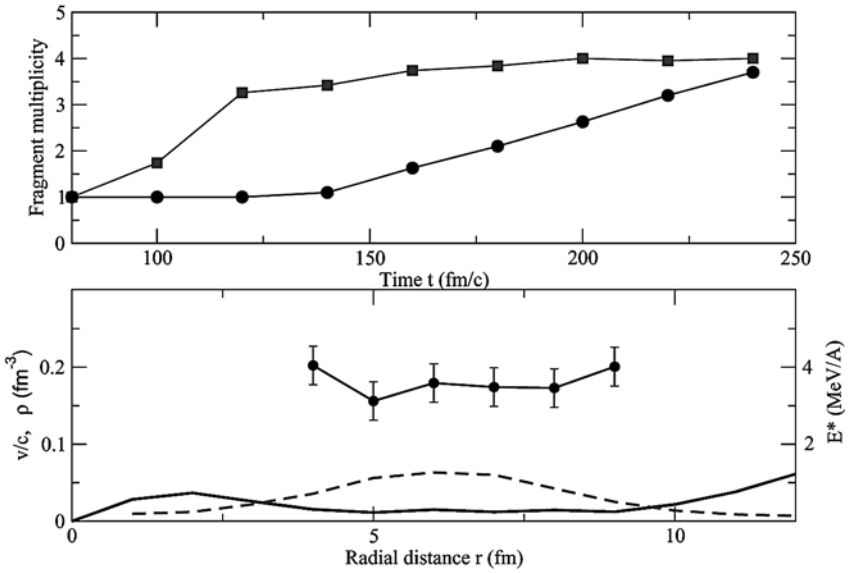

Fig. 11 – Dynamical results. Upper panel: Evolution of IMF (circles) and pre-fragment (squares) multiplicities in time. Lower panel: Collective velocity (full line), nuclear density (dashed line) and excitation energy per nucleon (circles), as a function of the distance from the center of mass of the system, corresponding to 140 fm/c. The excitation energy is evaluated in the region occupied by pre-fragments.

From the lower panel of Fig. 11 we also infer that the pre-fragments are formed near the turning point of the expansion. With increasing beam energy more radial flow is developed, the system expands in a hollow configuration and qualitatively different fragment partitions are dynamically populated [23].

D. REMARKS

One can conclude that, (for similar reactions) the experimental freeze-out volumes are relatively small (for the present reaction $3.4V_0$) and primary fragment excitation energy is considerably large (4.3 MeV/u for this case). So, one deals with *hot* fragmentation at *small* freeze-out volumes. Also, for the studied case, there is no need for a cut-off factor in the fragments' level density, the minimum *Err* being obtained for $\tau = \infty$. Finally, the formed compound system is completely equilibrated without any extra flow energy. The physical consistency of the obtained result confirms the accuracy of the MMM analysis. This analysis rigorously demonstrates (maybe for the first time) that in the dynamical paths of violent heavy ion collisions there is a stage of *complete statistical equilibration* of the compound system. It is remarkable that the equilibrated source obtained *only* by fitting fragment size distributions and fragment internal energies proves its physical consistency subject to the dynamical calculations. Indeed, after propagating the fragments from thefreezeout volume specific to the identified equilibrated source to the one corresponding to the dynamical events, both kinematic and fragment position observables fit the corresponding dynamical data very well. The equilibrated stage corresponding to a time of 140 fm/c was found to coincide with the prefragment saturation region.

VIII. SUMMARY

Statistical ensembles are quite suitable for the descriptions of the nuclear multifragmentation phenomenon. Due to the finite size of the systems and to the manifesting conservation laws the *microcanonical ensemble* is the appropriate instrument to study such systems. The Microcanonical Multifragmentation Model (MMM) sharply simulates the microcanonical ensemble associated with the physical phenomenon. This model proves to be a powerfull tool to get important physical information about the nuclear multifragmentation phenomenon. MMM provides excellent description of experimental multifragmentation data and predicts a first order phase transition in nuclear matter. This transition appears to depend on the value of Coulomb interaction energy in the systems under study: Coulomb energy lowers the position of the critical point of the system under study. Starting from the MMM microcanonical weights microcanonical heat capacity are deduced. These formulas are *universally* applicable to *any* system

for which the "external" degrees of freedom can be treated classically irrespective to other specificness of the system and can be (experimentally) used to identify possible first order phase transitions. Indeed, the system's spinodal region will be signaled by negative values of the heat capacity. Finally, a statistical analysis of the MMM model on the dynamical multifragmentation path of transport code SMF aiming to identify a possible equilibrated region was described. An equilibrated region corresponding to 140 fm/c and coinciding to the prefragment saturation number was uniquely identified. In this way, it was rigorously demonstrated that an equilibrated source can be indeed at the origin of nuclear multifragmentation. The equilibrated freeze-out appears to occur in a prefragment stage of the system, *i.e.* prior to complete formation and separation of the fragments when system's constituents are still in (strong) interaction. This contradicts the widely used equilibrated freeze-out association with a stage where fragments are completely formed and separated and invites towards refinements of concepts and models.

REFERENCES

1. G. Bertsch, P. J. Siemens, *Phys. Lett.*, B **126**, 9 (1983).
2. J. Pochodzalla *et al.*, *Phys. Rev. Lett.*, **75**, 1040 (1995).
3. D. H. E. Gross, *Rep. Progr. Phys*., **53**, 605 (1990).
4. J. P. Bondorf, A. S. Botvina, A. S. Iljinov, I. N. Mishustin, K. Sneppen, *Phys. Rep*., **257**, 133 (1995).
5. Al. H. Raduta, Ad. R. Raduta, *Phys. Rev.*, **C55**, 1344 (1997);
   Al. H. Raduta, Ad. R. Raduta, *Phys. Rev.*, **C61**, 034611 (2000).
6. J. Randrup, S. Koonin, *Nucl. Phys.*, **A471**, 355c (1987).
7. J. D. Frankland *et al.*, *Nucl. Phys.*, **A689**, 905 (2001).
8. J. D. Frankland *et al.*, *Nucl. Phys.*, **A689**, 940 (2001).
9. J. Randrup, *Comput. Phys. Commun.*, **59**, 439 (1990).
10. Al. H. Raduta, Ad. R. Raduta, *Phys. Rev.*, C **61**, 034611 (2000).
11. G. Fai, J. Randrup, *Nucl. Phys.*, **A381**, 557 (1982).
12. Al. H. Raduta, *Nucl. Phys.*, **A683**, 618 (2001).
13. F. Gulminelli, Ph. Chomaz, *Nucl. Phys.*, **A734**, 581 (2004).
14. Al. H. Raduta, Ad. R. Raduta, *Phys. Rev.*, **C65**, 054610 (2002).
15. Al. H. Raduta, Ad. R. Raduta, *Nucl. Phys.*, **A647**, 12 (1999).
16. Al. H. Raduta, Ad. R. Raduta, *Phys. Rev.* Lett., **87**, 202701 (2001).
17. F. Gulminelli, Ph. Chomaz, V. Duflot, *Europhys. Lett*., **50**, 434 (2000).
18. Al. H. Raduta, Ad. R. Raduta, *Nucl. Phys.*, **703**, 876 (2002)
19. Ph. Chomaz, F. Gulminelli, *Nucl. Phys.*, **A647**, 153 (1999).
20. M. D'Agostino *et al.*, *Phys. Lett*., **B 473**, 219 (2000).
21. J.P.Bondorf *et al.*, *Phys. Rev. Lett*., **B 473**, 628 (1994).
22. J.D. Frankland *et al.*, *Nucl. Phys.*, **A689**, 940 (2001).
    G. Tabacaru *et al.*, *Eur. Phys. J.*, **A18**, 103 (2003).
23. M. Colonna, G. Fabbri, M. Di Toro, F. Matera, H. H. Wolter, *Nucl. Phys.*, **A742**, 337 (2004).

24. A. H. Raduta, M. Colonna, V. Baran, M. Di Toro, *Phys. Rev.*, C **74**, 034604 (2006).
25. M. Colonna *et al.*, *Nucl. Phys.*, **A642**, 449 (1998).
26. Ph. Chomaz, M. Colonna, J. Randrup, *Phys. Rep*., **389**, 263 (2004).
27. A. Guarnera *et al.*, *Phys. Lett.*, **B403**, 191 (1997).
28. C. O. Dorso, J. Randrup, *Phys. Lett*., **B301**, 328 (1993).
29. M. Parlog *et al.*, *Eur. Phys. J.*, **A25**, 223 (2005).